J. Fluid Mech. (1978), *vol.* 87, *part* 3, *pp.* 561–582
Printed in Great Britain

The numerical simulation of wind–wave interaction

By D. V. CHALIKOV

Leningrad Branch, P. P. Shirshov Institute of Oceanography,
USSR Academy of Sciences, 30 Pervaya Liniya, Leningrad 199053, USSR

(Received 20 May 1977 and in revised form 17 November 1977)

The Navier–Stokes equations for a two-layer flow are written in a curvilinear system of co-ordinates in which the height is measured from the interface. A technique for averaging the equations over an ensemble of wave surfaces which are not very different from each other is proposed. Moments which include deviations in the rate of surface displacement and in the slopes are dropped. It is assumed that the averaged equations describe the evolution of a large-scale velocity field. The moments of the turbulent velocity field are parameterized using the isotropic coefficient of turbulent viscosity, which, from dimensional considerations, is expressed in terms of the length scale growing linearly upwards and downwards from the interface and the turbulent kinetic energy. The equation defining the evolution of turbulent energy is derived without allowing for the curvilinearity of the system of co-ordinates. Laboratory experiments in a wind–water tunnel are simulated by integrating the equations numerically. The results are compared with measurements.

1. Introduction

Wind waves are one of the most thoroughly studied natural hydrodynamic phenomena. They are adequately covered by experimental data and in many ways have been effectively simulated for laboratory conditions. The theory of wind waves is a highly developed division of geophysical fluid dynamics and the theories relevant to the generation and growth of waves presented by Phillips (1957) and Miles (1957) are its most important results. These theories give a clear qualitative interpretation of the mechanisms of wave energy exchange and are in satisfactory agreement with experimental data (Barnett & Kenyon 1975). Certainly, these two theoretical studies and subsequent results of this kind have been obtained using a number of simplifications of which the most significant is the assumption that the amplitudes are small. In certain respects, this assumption immediately leads to contradictions. For example, in many interesting cases, the height of the critical layer appears to be smaller than the wave height. In such situations the mechanism of wave energy exchange acts somewhere between the trough and crest of a finite amplitude wave. Rejection of the hypothesis of small amplitudes imposes a restriction on the applicability of analytical studies, so that numerical simulation remains the most effective tool available.

Numerical simulation has recently led to remarkable progress in many divisions of geophysical fluid dynamics. Indeed it seems astonishing that numerical solution of the complete equations has not been applied to the simulation of wind–wave interaction. The reason for this becomes clear, however, as one goes deeper into the subject because there appear to be many obstacles involved in constructing a mathematical

model which describes this phenomenon. Most important of these is certainly the ambiguity arising in an attempt to average the equations of motion for a two-layer turbulent fluid. This procedure requires parameterization of the inner turbulence and 'interface turbulence' and the way to do this is not obvious. In particular, it seems to be very difficult to include the mechanisms of resonant interaction (Phillips 1957).

This paper is concerned with one of the possible averaging procedures. Another problem which requires solution is how to select a way to close the equations, i.e. parameterize the inner turbulence and 'interface turbulence'. To date, there seems to be no reason to prefer any particular method, therefore here, as in Gent & Taylor (1976), the simplest method has been chosen, that based on the equation of turbulent energy balance. It appears that the general approach involving the solution to the complete equations may subsequently reveal which of the methods is the best.

The numerical results given in this paper are relevant to the case of two-dimensional waves. This approximation is satisfactory for many laboratory experiments. Simulation of a real, three-dimensional flow is not difficult in principle, but requires a computer with a very large capacity. The difficulties in constructing a good numerical scheme which permits simulation of the accumulation of energy in waves may be not of primary importance but they could be a significant obstacle to a direct numerical simulation. In any case, the computational effort required in this problem may be too great for present-day machines.

The purpose of this paper is to discuss an approach to the mathematical simulation of the water–air layer involved in wind–wave interaction (see also Chalikov 1976).

2. The basic equations: the ζ co-ordinate

The main difficulty in deriving the dynamic equations for a medium involving a density discontinuity across a surface is that averaging is impossible in an Eulerian system of co-ordinates. This difficulty vanishes if the vertical co-ordinate ζ is measured from the interface rather than a fixed level, i.e.

$$\zeta = z - \eta, \tag{1}$$

where z is the height relative to the mean level and η is the elevation. In terms of ζ, the Navier–Stokes equations take the form

$$u_t + (uu)_x + (vu)_y + (wu - \eta_t u - \eta_x uu - \eta_y uv)_\zeta = -\rho^{-1}P_x + \rho^{-1}\eta_x P_\zeta + \nu\Delta u, \tag{2a}$$

$$v_t + (uv)_x + (vv)_y + (wv - \eta_t v - \eta_x uv - \eta_y vv)_\zeta = -\rho^{-1}P_x + \rho^{-1}\eta_y P_\zeta + \nu\Delta v, \tag{2b}$$

$$w_t + (uw)_x + (vw)_y + (ww - \eta_t w - \eta_x uw - \eta_y vw)_\zeta = -\rho^{-1}P_\zeta + g + \nu\Delta w, \tag{2c}$$

$$u_x + v_y + (w - \eta_x u - \eta_y v)_\zeta = 0, \tag{2d}$$

where u, v and w are the longitudinal (x), transverse (y) and vertical (ζ) velocity components, ρ is the density ($\rho = \rho_a$, the air density, in $\zeta > 0$ and $\rho = \rho_w$, the water density, in $\zeta < 0$), ν is the molecular viscosity, P is the pressure and Δ is the Laplacian in the co-ordinate system (x, y, ζ). The following kinematic condition is added to (2):

$$h_t = w_0 - u_0\eta_x - v_0\eta_y, \tag{3}$$

where u_0, v_0 and w_0 are the velocity components at the surface $\zeta = 0$. Equation (3) indicates that there is no mass, momentum or energy exchange through the interface due to advective terms: on the left-hand sides of (2*a–d*) the groups of terms

differentiated with respect to ζ reduce to zero. It follows that the energy and momentum fluxes through the interface are effected by the forces due to pressure and viscosity alone. Note that, if the continuity of the interface is violated, (3) is inapplicable and the two media can exchange finite volumes in the form of air bubbles and spray. This may take place when the interface becomes unstable. The transition to instability is identical to that for laminar flow because in both cases molecular exchange is replaced by the exchange of finite volumes.

3. Averaging of the equations: the wind–wave interaction layer

In terms of ζ, particles with equal heights always belong to the same medium, so that formally no difficulties arise at the interface. Consider a certain horizontal scale l_r and separate the spectrum of perturbations into large-scale components with horizontal scales $\lambda > l_r$ and small-scale components $\lambda < l_r$. The problem consists of constructing equations which describe the motions with scales $\lambda > l_r$ but allow for the statistical influence which the small-scale components exert on them. When applied to numerical realization of the model when l_r is identified with one or several steps of the finite-difference grid, the method of calculating the effects of small-scale motions on terms describing explicitly the influence of large-scale motions forms the so-called problem of subgrid-effect parameterization. With respect to the variable $\eta(x, y, t)$, the scale separates out waves with horizontal dimensions $\lambda > l_r$, whose motion is defined by averaged equations. Where the waves have length $\lambda < l_r$, their heights, from *a priori* considerations or experimental data, may be assigned an approximate value h_r. The value of h_r may be estimated more satisfactorily if l_r is sufficiently small and the subgrid waves belong to the high frequency subrange where universal laws hold with some accuracy for the elevation and slope spectra. It is not difficult to establish from dimensional considerations that if l_r lies in the inertial range, then h_r is directly proportional to l_r and is independent of time and the spatial co-ordinates.

We now define the ensemble which will be used in averaging. Consider a domain G whose horizontal dimensions are larger than the maximum length of a wave and which is bounded above by the surface $\zeta = H_a$ and below by the surface $\zeta = -H_w$. Here H_a is higher than the levels where it is possible to trace the velocity and pressure perturbation fields propagating away from the surface. The observations appear to indicate that H_a may be taken equal to several heights of the maximum wave. Nevertheless, we shall assume that the lower and upper boundaries both lie at a distance of one maximum wavelength from the interface. We shall call the layer bounded by the surfaces $\zeta = H_a$ and $\zeta = -H_w$ the wind–wave interaction layer.

Examine the set of realizations of a two-layer turbulent flow in the region G for similar external conditions (such as the time of occurrence, the mean-wind direction and the velocity beyond the layer of wind–wave interaction). To collect an ensemble of realizations to be used in averaging, it will be necessary that, for any two representatives of this ensemble I and II, the surfaces $\eta_{\mathrm{I}}(x, y)$ and $\eta_{\mathrm{II}}(x, y)$ coincide with each other to within a distance h_r:

$$\max |\eta_{\mathrm{I}}(x, y) - \eta_{\mathrm{II}}(x, y)| \lesssim h_r, \tag{4}$$

where, as specified above, h_r is consistant with l_r. Let $\overline{u}$, $\overline{w}$, $\overline{\eta}$ and $\overline{P}$ be the ensemble-averaged quantities and u', w', η' and P' their variations. It is natural that $\overline{u}$, $\overline{w}$ and

$\overline{P}$ should describe the effect of a smoothed wave surface $\overline{\eta}$ whereas u', w' and P' should correspond to the deviations due to (i) the turbulence in the internal velocity field and (ii) the high frequency components η' with scales $\lambda < l_r$. It should be emphasized that the averaging is performed with respect to ζ, i.e. over heights equi-distant from the interface. Averaging is also performed with respect to the vertical co-ordinate, with the result that for the averaged set of equations the height is measured from a smoothed surface. The method of averaging proposed here is, in effect, close to y-averaging (along the crests of two-dimensional waves) or phase averaging, but it takes into account the three-dimensional perturbations and the presence of a wave spectrum. We shall call this method G-averaging for brevity.

To reduce the computational effort, we shall suppose that the perturbations are quasi-two-dimensional. This means that three-dimensionality occurs on the small scales $\lambda < l_r$ alone. Let the direction of motion of these two-dimensional perturbations coincide with the mean-wind direction beyond the wind–wave interaction layer. Let the x axis be parallel to this mean wind and assume that all probability distribution functions for the deviations u', w', p' and η' are invariant with respect to shear and reflexion along the y axis. After averaging, the equations will take the form

$$\overline{u}_t + (\overline{u}\overline{u} + \overline{u'u'})_x + (\overline{w}\overline{u} + \overline{w'u'} - \overline{\eta}_t\overline{u} - \overline{\eta}_x\overline{u}\overline{u} - \eta_x\overline{u'u'})_\zeta = -\rho^{-1}\overline{P}_x + \rho^{-1}\overline{\eta}_x\overline{P}_\zeta + M_u, \quad (5a)$$

$$\overline{w}_t + (\overline{u}\overline{w} + \overline{u'w'})_x + (\overline{w}\overline{w} + \overline{w'w'} - \overline{\eta}_t\overline{w} - \overline{\eta}_x\overline{u}\overline{w} - \overline{\eta}_x\overline{u'w'})_\zeta = -\rho^{-1}\overline{P}_\zeta + g + M_w, \quad (5b)$$

$$\overline{u}_x + (\overline{w} - \overline{\eta}_x\overline{u} - \overline{\eta'_x u'})_\zeta = 0, \quad (5c)$$

$$\overline{\eta}_t = \overline{w}_0 - \overline{u}_0\overline{\eta}_x - \overline{u'_0\eta'_x}, \quad (5d)$$

where the terms defining the molecular viscosity have been omitted. M_u and M_w indicate the sums of the second and third moments including η'_x or η'_t. These moments, as well as the last terms on the left-hand sides of (5a–c), may be considered to decrease with increasing distance from the surface just as two-point moments decrease with increasing distance between the points. The rate of their reduction depends on the spectral radius of correlation R_r, which may be determined from the discretization scales l_r and h_r. Since l_r and h_r are taken to be small, it is possible to assume that the layer wherein M_u and M_w make a significant contribution is rather thin. It appears that, as in the case of large-scale components, the perturbations due to high frequency waves are attenuated at a height several times the height of these waves for $\zeta > 0$ and at a depth of order l_r for $\zeta < 0$. The difference between the attenuation rates above and below the interface may be due to the fact that in the air intensive turbulence blurs the surface-generated perturbations, whereas in the water the motion is nearly potential and turbulent energy is appreciably smaller (unless intensive wave breaking occurs). To date, no experimental data are available for estimating the radius of correlation R_r.

We note that a layer wherein the velocity and pressure fields are correlated with the surface slope also occurs above an ordinary rough surface in the vicinity of the roughness elements. Henceforth it will be assumed that the high frequency surface-generated perturbations affect the flow in the same way as surface elements. These perturbations will thus be taken into account in formulating the resistance law.

The depth of the layer of interaction with waves of length $\lambda < l_r$ can be roughly estimated in the following manner. Let the spectrum of elevations at high frequencies

be described by Phillips' (1958) formula $S(\omega) = \beta g^2 \omega^{-5}$ and the spectrum of slopes by the formula $S'(\omega) = \alpha\omega^{-1}$ (Phillips 1966, p. 109). Then, assuming that

$$l_r \sim 2\pi S^{\frac{1}{2}}(\omega_r)\,[S'(\omega_r)]^{-\frac{1}{2}}, \quad h_r \sim \left(\int_{\omega_r}^{\infty} S(\omega')\,d\omega'\right)^{\frac{1}{2}},$$

it is possible to estimate the minimum frequency ω_r and typical height of the waves which are not taken into account explicitly:

$$\omega_r \sim (2\pi)^{\frac{1}{2}}(\beta/\alpha)^{\frac{1}{4}} g^{\frac{1}{2}} l_r^{-\frac{1}{2}}, \quad h_r \sim (4\pi)^{-1}\alpha^{\frac{1}{2}} l_r. \tag{6}$$

If the horizontal scale of discretization l_r is taken to be 10 cm, then it follows from (6) that, for $\beta = 0{\cdot}5 \times 10^{-2}$ and $\alpha = 0{\cdot}8 \times 10^{-2}$ (Kitaigorodsky 1970, p. 200), $\omega_r \sim 25\,\mathrm{s}^{-1}$ and $h_r \sim 0{\cdot}5$ cm. In this case, the depth h_S of the layer wherein the terms M_u and M_w may be significant appears to be several centimetres. This permits the assumption that for simulating the dynamic structure of the interaction layer the terms M_u and M_w are insignificant everywhere except in a thin layer near the surface. This layer will be described later in this paper.

The height of propagation of the perturbations due to waves of frequency $\omega < \omega_r$ increases as ω decreases and may be appreciably larger than h_S, but these perturbations are then described explicitly by (5). In principle, for waves of any frequency it is possible to find the heights ζ where the correlation of the velocity and pressure fields with the surface slopes becomes negligibly small. In particular, $\zeta = H_a$ and $\zeta = -H_w$ are defined as levels at which this correlation is zero for all perturbation frequencies. Beyond the layer of interaction, there exists a simple relationship between single-point moments calculated in the ζ and usual co-ordinates respectively:

$$\tilde{m}(\zeta) = \int_{-\infty}^{\infty} m(z-\eta')\,p(\eta')\,d\eta', \tag{7}$$

where m is any single-point moment at a height z, $\tilde{m}$ is the same moment at ζ and $\rho(\eta)$ is the probability distribution function of surface elevations.

It follows from (7) that if m changes slowly enough with height the difference between z and ζ may be neglected beyond the layer of interaction.

4. Parameterization of the subgrid processes

For the ultimate formulation of the problem, the system (5) must be closed. Later we shall present the closure used in the calculations. This may not be the best scheme because it was selected under the restriction that the computing time required should be acceptable.

Turbulence

The second-order single-point moments can be parameterized in terms of the deformation tensor of the mean velocity field and the coefficient of turbulent viscosity k, which is expressed in terms of the kinetic turbulent energy $e = \frac{1}{2}(\overline{u'^2}+\overline{v'^2}+\overline{w'^2})$ and the turbulence scale l using the hypothesis

$$k = (e/c)^{\frac{1}{2}} l. \tag{8}$$

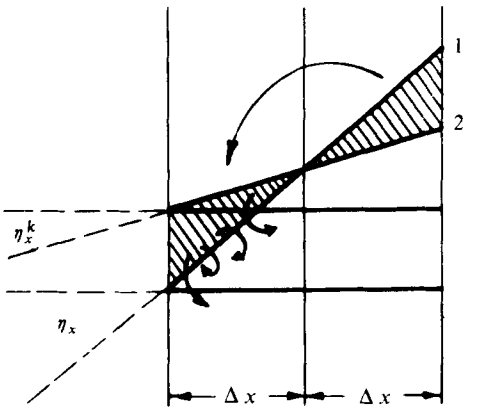

FIGURE 1. Diagram explaining the process of wave breaking. η_x is the surface slope before breaking while η_x^k is that after wave breaking. The displacing volume is shaded. The arrow shows the direction of displacement.

As the simplest assumption, l can be taken to be isotropic and growing linearly with increasing distance from the interface:

$$l = \kappa|\zeta| \tag{9}$$

($\kappa = 0{\cdot}4$ is the von Kármán constant). To effect system closure with ζ defined as in (1), a standard technique is used to derive an equation of turbulent energy evolution (Monin & Yaglom 1971, chap. 3). The technique used to describe turbulence in the model presented below was appreciably simplified [see (8)].

Decreasing potential energy

The foregoing discussion of the moments which include derivatives of the deviation in the surface level is certainly inapplicable to the value the moment $\overline{u_0'\eta_x'}$ at the surface itself. This term describes the effect of high frequency variations on low frequency variations. It is possible to assume that at least at high frequencies $\omega > \omega_r$ potential energy flows more effectively from low to high frequencies than vice versa. From the point of view of energetics, this effect produces a non-reversible decrease in the potential energy of the individual perturbation components. For sufficiently well developed perturbations this decrease may appear as wave breaking. A suitable differential form for the term $\overline{u_0'\eta_x'}$ might be $k_\eta \overline{\eta}_{xx}$, where k_η is a smoothing coefficient. A defect in this form is its low selectivity with respect to surface slopes. The smoothing, apparently, must act on sufficiently large slopes and be absent altogether for small slopes. This defect can be rectified by making k_η increase with $\overline{\eta}_x$. The simplest method of parameterizing wave breaking which is suitable for numerical simulation is to prevent the inception of an excessively large local steepness $\overline{\eta}_x$. It is supposed that, once the steepness exceeds some critical value η_x^k, the supercritical volume of fluid breaks in the direction of the reduction in level (figure 1) and all the rising potential energy changes into turbulent energy. It is not difficult to calculate that the vertical turbulent energy flux in this system is

$$\Pi = \rho_w g(\Delta x)^2 (6\Delta t)^{-1} [\eta_x^2 - (\eta_x^k)^2], \tag{10}$$

where Δx is the horizontal step and Δt is the time step of the numerical model. If waves with an angle of about 120° at the crest are considered critical, then the estimate $\eta_x^k \sim 3^{-\frac{1}{2}}$ holds. This method of estimating η_x^k and also the entire proposed parameterization of wave breaking cannot be accepted as final recommendations. Certainly, the initial phase of the inception of instability is described by (5*a–d*) themselves, but precisely these situations must be eliminated, otherwise a computational instability explodes.

An alternative criterion for defining the interface instability is to compare the local vertical acceleration w_t with gravitational acceleration g.

Interface and bottom friction

The coefficient of turbulent viscosity at $\zeta = 0$ reduces to zero owing to (9). Nevertheless, at the surface tangential friction τ_S does exist. We assume that this friction is proportional to the square of the local tangential velocity. Since the friction forces acting on the surface from above and from below are equal, it is easy to obtain

$$\tau_S = \rho_a \Delta u_\tau |\Delta u_\tau| C_S, \tag{11}$$

where $\Delta u_\tau = (u^+ - u^-) + \eta_x(w^+ - w^-)$ ($u^\pm$ and $w^\pm$ are the velocity components immediately above and below the interface respectively). A very simple assumption which can be made here is that the local tangential velocity profile above the interface is described by the logarithmic law. This leads to

$$C_S = \kappa^2 [\ln (z^+/z_0)]^{-2}, \tag{12}$$

where z_0 is the interface roughness parameter and z^+ is the height corresponding to the velocity (u^+, w^+). For such a simple resistance model, the local roughness of the water surface under natural conditions is produced by high frequency wave components whose phase velocity is usually much smaller than the local air velocity. Assume that z_0 is determined by the characteristic height of these waves (Kitaigorodsky 1970, p. 46):

$$z_0 = \tfrac{1}{30} h_r. \tag{13}$$

If ω_r belongs to the inertial subrange, then it follows from (6) that $z_0 \sim \frac{1}{60}\alpha^{-1} l_r$.

Parameterization of the surface friction on the basis of the proposed assumptions reduces to the transformation

$$\rho k u_\zeta|_{\zeta=\pm 0} \to \tau_S, \quad \rho k w_\zeta|_{\zeta=\pm 0} \to \eta_x \tau_S, \tag{14}$$

which ensures continuity of the tangential force across the interface.

Simulation of laboratory experiments often permits the assumption of a smooth water surface and the use of the approximation

$$z_0 = m_0 \nu (\tau_S/\rho_a)^{-\frac{1}{2}}, \tag{15}$$

where m_0 is a constant of order 10^{-1}.

To realize a steady solution for the mean longitudinal velocity, this component is assumed to decay at the lower boundary of the domain. To be specific, it is supposed that a little below the level $z = -H_w$ there is the bottom boundary layer. The bottom friction $k u_\zeta|_{\zeta=-H_w}$ is calculated from the formula

$$\tau_b = k u_\zeta|_{\zeta=-H_w} = u_b |u_b| C_b, \tag{16}$$

where C_b is the usual resistance coefficient above a rough surface and u_b is the longitudinal bottom velocity. The case of finite depth has been chosen for simplicity. In deep water, we are obliged to take the Coriolis force into account or to parameterize the developing Ekman layer.

Turbulent energy influx due to wave breaking

Neglecting the turbulent energy production at high frequency surface elements generally leads to the relation $ke_\zeta = 0$ for $\zeta = 0$. This relation, however, should be used only above the interface. Below it there occurs a vertical flux e induced by wave breaking:

$$ke_\zeta|_{\zeta=+0} = 0, \quad ke_\zeta|_{\zeta=-0} = \rho_w^{-1}\Pi. \tag{17}$$

It should be emphasized that these assumptions are not very accurate because they do not allow for direct turbulence production due to the work done on the high frequency waves by frictional and pressure forces.

Model equations and boundary conditions

Since the method of describing the effects of eddy viscosity, which is based on (8), (9) and the equation for the evolution of the turbulent kinetic energy, is not very accurate, we drop some terms in the equation of motion and the terms due to transition to the ζ co-ordinate in the equation for e. These simplifications arising from the considerations of numerical reality can be made only on the assumption that the ratio of the vertical and horizontal perturbation scales is sufficiently small. The set of equations finally takes the form (the averaging sign is left out)

$$u_t = (-uu - \rho^{-1}p + ku_x + g_1\eta)_x + (-uw + \eta_t u + \eta_x uu + \eta_x\rho^{-1}p + ku_\zeta)_\zeta, \tag{18a}$$

$$w_t = (-uw + kw_x)_x + (-ww + \eta_t w + \eta_x uw - \rho^{-1}p + kw_\zeta)_\zeta, \tag{18b}$$

$$u_x + (w - \eta_x u)_\zeta = 0, \tag{18c}$$

$$\eta_t = w_0 - u_0\eta_x - \overline{u_0'\eta_x'}. \tag{18d}$$

Here the net pressure is replaced by its deviation from the hydrostatic component

$$p = P - g\int_\zeta^{H_a} \rho\, dz + g\rho_a\eta \tag{19}$$

and

$$g_1 = \begin{cases} 0 & \text{for} \quad \zeta \geqslant 0, \\ g(1-\rho_a\rho_w^{-1}) & \text{for} \quad \zeta < 0. \end{cases} \tag{20}$$

Equations (18) are used together with the evolution equation for the turbulent energy:

$$e_t = (-ue + ke_x)_x + (-we + \eta_t e + \eta_x ue + ke_\zeta)_\zeta + k(u_x^2 + u_\zeta^2 + w_x^2 + w_\zeta^2) - \epsilon, \tag{21}$$

where the dissipation ϵ, like k [see (8)], is expressed in terms of e and l:

$$\epsilon = (e/c)^{\frac{3}{2}} l^{-1} \tag{22}$$

($c = 4{\cdot}6$ is an empirical constant, see Zilitinkevich 1970, p. 106). The above simplifications are relevant only to the terms which involve the turbulent viscosity. It seems inconsistent to retain the small terms when the description of turbulence is so in-

accurate. Computations indicate that these simplifications in fact have little influence on the results.

The set of equations (18) and (21) may be solved in a 'rectangular' region with horizontal length L and height $H_a + H_w$. Along the x axis, we assume periodicity with period L of all unknown functions and the required derivatives. This means that we take into account only the waves with length L/n, where n is an integer. This constraint is inevitable in modelling a real process. Simulation of laboratory experiments may involve modelling real boundary conditions, but this will increase the amount of computation considerably.

At the upper boundary of the region we assign a turbulent momentum flux τ and a turbulent energy defined by τ and also assume vanishing of the vertical velocity and pressure perturbations:

$$ku_\zeta = \rho_a^{-1}\tau, \quad e = c\rho_a^{-1}, \quad w = 0, \quad p = 0 \quad \text{at} \quad \zeta = H_a. \tag{23}$$

At the lower boundary the velocity perturbations vanish and we assign a turbulent energy defined by a turbulent momentum flux τ_b:

$$u = 0, \quad w = 0, \quad e = c\tau_b \quad \text{at} \quad \zeta = -H_w. \tag{24}$$

The pressure p can be obtained by solving a second-order equation (of the elliptical type). Therefore at the lower boundary of the region $\zeta = -H_w$ yet another boundary condition, for P, is obtained through substitution of (14) into a finite-difference analogue of (18).

5. Vertical flux of momentum and energy

Considering the air flow to be quasi-steady, we average (18a) over the interval $(0, L)$ to obtain

$$\overline{(p\eta_x - uu + \eta_t u + \eta_x uu + ku_\zeta)_\zeta} = 0. \tag{25}$$

The sum within the brackets is independent of the height in the layer $(0, H_a)$. The first four terms in (25) decrease with height and for $\zeta > H_a$ there remains the term ku_ζ, which is equal to the moment $\overline{u'w'}$ calculated in terms of ζ. According to (7), this moment is equal to that found at a fixed value of z, i.e. to frictional stresses in the usual sense. After substitution of the vertical velocity $\tilde{w} = w - \eta_t - \eta_x u$ measured from the interface, (25) can be written in the form

$$\overline{p\eta_x} - \overline{\tilde{w}u} + \overline{ku_\zeta} = \tau. \tag{26}$$

It is clear that the vertical momentum flux in terms of ζ is due to the pressure forces, the velocity field (to be described individually) and the eddy viscosity. Taking into account the kinematic conditions $\tilde{w} = 0$ and $ku_\zeta = \tau_S$ at the interface, so that momentum is transferred to the water only by pressure forces and surface friction, we obtain

$$\overline{p\eta_x} + \bar{\tau}_S = \tau \quad \text{at} \quad \zeta = 0. \tag{27}$$

If air flow is assumed to be quasi-steady and homogeneous, (18) can also be used to obtain the formula for the energy flux W_0 through the interface:

$$W_0 = \overline{p\eta_t} + \overline{u_0\tau_S} + \overline{w_0\eta_x\tau_S}, \tag{28}$$

where the first term corresponds to energy transport by the vertical pressure forces, whereas the second and third terms are due to tangential friction.

The contribution of each term to (26), (27) and (28) may vary depending on the resolution adopted. Therefore the question of the contributions of normal and tangential forces and two methods of energy transfer from one medium to the other in the presence of the perturbation spectrum cannot be addressed without specifying the boundaries of spectral intervals.

6. Example of the numerical calculations

The proposed set of equations is intended for calculating the evolution of wind-induced waves. This major task requires that very stringent demands on the accuracy of the finite-difference scheme be met and involves much computer time. A possible method of testing the feasability of the model with a smaller amount of computations is to simulate laboratory experiments. For this purpose, we have assembled data from the laboratory experiments by Stewart (1970), who measured the velocity distribution in a wind–water tunnel over waves with a wavelength $L = 40{\cdot}8$ cm and a height $a = 0{\cdot}64$ cm. The water depth was 21 cm, the phase velocity $C_\eta = 79{\cdot}6$ cm/s and the wavenumber $k = 0{\cdot}155$ cm^{-1}. It required 3·5 s for a wave to travel the 274 cm distance from the wave maker to the instruments. Over this distance there occurred above the waves a boundary layer with a height of about 8 cm, wherein measurements were made. Stewart confined himself to the study of wave-induced perturbations in the air flow above waves. The simplest way to simulate this experiment might be to solve (18) and (21) above a water–wave surface. However, from technical considerations, we preferred to solve a general problem for a two-layer fluid including (18) and (21) supplemented by the hypotheses (8), (9), (11), (16) and (22) with boundary conditions (23) and (24). The length of the integration area was selected to be equal to the wavelength, the height H_a above the surface in different versions was taken to be from 10 to 15 cm and the depth was 15 cm (see table 1). At the beginning we introduced one travelling wave using the formulae of small amplitude wave theory and a logarithmic velocity distribution in the upper region. The waves in Stewart's experiment were almost smooth. In this case, the effective roughness is due to the processes in a viscous sublayer, which requires much supplementary effort if it is to be simulated in the framework of the present model. Therefore the roughness parameter here was estimated using (15) with the coefficient $m_0 = 0{\cdot}23$ defined from Stewart's profile measurements.

For 1–2 s, mutual relaxation of the velocity and pressure fields occurred, whereupon the picture involved waves with certain fluctuations. Despite the small integration time, the amount of computation in this problem was rather large. This was caused partly by the comparatively small time step (from 0·001 to 0·01 s) used in the computations but mainly by the necessity to solve an elliptical equation for the pressure at each step. During the integration period (usually 5·1 s) the net energy, which was equal to the sum of the kinetic energy

$$E_k = \frac{1}{2L}\int_0^L \int_{H_w}^{H_a} \rho(u^2+w^2)\,d\zeta dx$$

and the potential energy

$$E_p = \frac{g\rho_w}{2L}\int_0^L \eta^2 dx,$$

	$v_* = 3{\cdot}36$ cm/s	$v_* = 6{\cdot}71$ cm/s	$v_* = 8{\cdot}33$ cm/s
Horizontal step (cm)	4·08	2·04	2·04
Number of nodes along horizontal	10	20	20
Vertical step (cm)	1	0·5	0·5
Height H_a (cm)	15	10	10
Number of levels in air	15	20	20
Depth H_w (cm)	15	15	15
Number of levels in water	15	30	30
Time step (s)	0·01	0·00125	0·001
Wave phase velocity (cm/s)	78·6	79·4	80·1
Potential energy (erg/cm^2)			
$t = 0$ s	101	100	100
$t = 2{\cdot}5$ s	93	93	91
$t = 5{\cdot}0$ s	97	88	86
Kinetic energy (erg/cm^2)			
$t = 0$ s	127	174	227
$t = 2{\cdot}5$ s	136	174	227
$t = 5{\cdot}0$ s	130	164	215

TABLE 1

decreased by several per cent (see figure 2). Apparently, this reduction is largely due to the dissipative character of the scheme. The wave shape was conserved with a high degree of accuracy. This is illustrated in figure 3, which presents wave spectra for two times. It is clear that, as in Stewart's experiment, practically all of the energy is contained in the dominant mode. Certainly, the waves were far from breaking in all versions of the calculation.

An attempt has been made to simulate wave evolution for $v_* = 3{\cdot}36$ cm/s by integrating the set of equations over a period of 60 s (this required 6000 time steps). Here the wave energy slowly decreased, but the general picture remained unchanged. Unfortunately, the errors involved in approximating the time derivatives in all cases obscured natural accumulation of the wave energy. The wave phase velocity, which is controlled by the velocity of crest displacement, coincided to a very good accuracy with the experimental value regardless of the wind velocity and method of integration with respect to time, the deviations usually being within 1%.

After 1–2 s, the structure of disturbance in the air also remained approximately the same. This is illustrated in figure 4, which gives the distribution of the amplitudes $\mathscr{U}$ and $\mathscr{W}$ of the wave-induced perturbations in the air normalized by av_*^2/ν *vs.* the wavenumber k for $v_* = 8{\cdot}33$ cm/s. The curves apply to different heights with respect to the mean level. Transition from the ζ to the z co-ordinate was performed using linear interpolation. The two sets of curves obtained for different times are somewhat different in detail, but the resemblance between them is obvious. The longitudinal velocity profiles above the waves together with Stewart's experimental data are shown in figure 5, which indicates that the shape of the profiles and the character of their differences for the trough and crest of a wave were simulated fairly satisfactorily.

If, on average, the air flow does not accelerate, then the net momentum flux due to the wave velocity components, pressure and eddy viscosity [equation (26)] must be independent of ζ. The instantaneous profiles of these quantities for $v_* = 8{\cdot}33$ cm/s are given in figure 6 (the positive values correspond to a downward momentum flux).

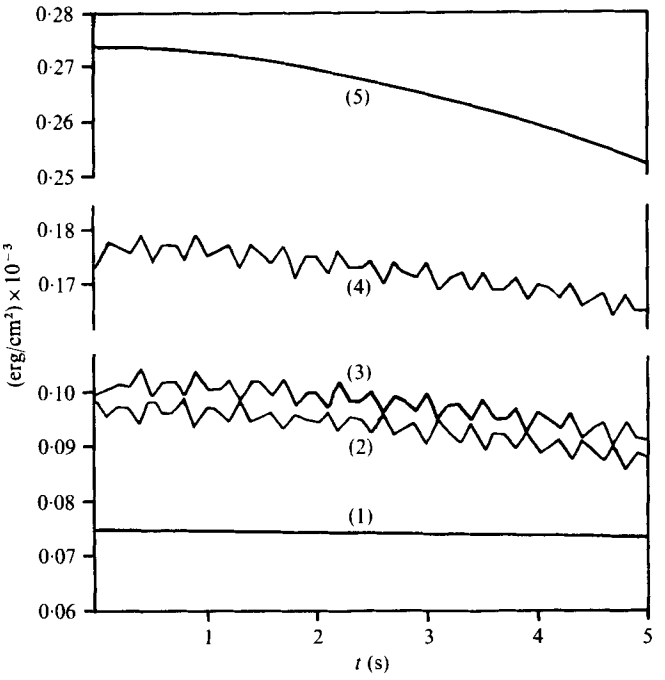

FIGURE 2. The time evolution of the energy components (erg/cm²) for $v_* = 6{\cdot}71$ cm/s. (1) Kinetic energy in the air, $E_\kappa^a = \dfrac{\rho_a}{2L}\int_0^L\int_0^{H_a}(u^2+w^2)\,d\zeta dx$. (2) Potential wave energy,

$$E_p = \frac{g\rho_w}{2L}\int_0^L \eta^2\,dx.$$

(3) Kinetic energy in the water, $E_\kappa^w = \dfrac{\rho_w}{2L}\int_0^L\int_{H_w}^0 (u^2+w^2)\,d\zeta dx$. (4) Net kinetic energy $E_k = E_k^a + E_k^*$. (5) Net energy $E = E + E$.

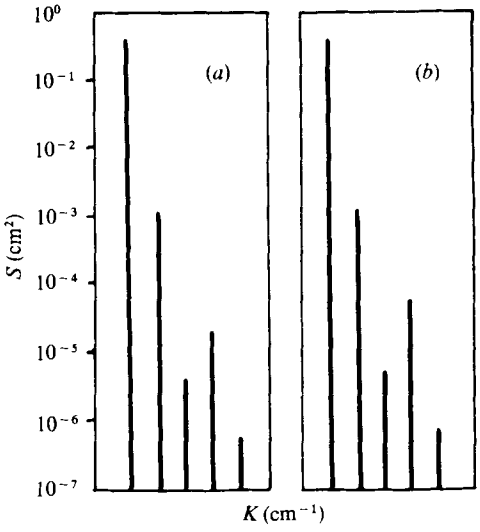

FIGURE 3. Wave spectra for $v_* = 3{\cdot}36$ cm/s.
(a) $t = 2{\cdot}0$ s, (b) $t = 4{\cdot}0$ s.

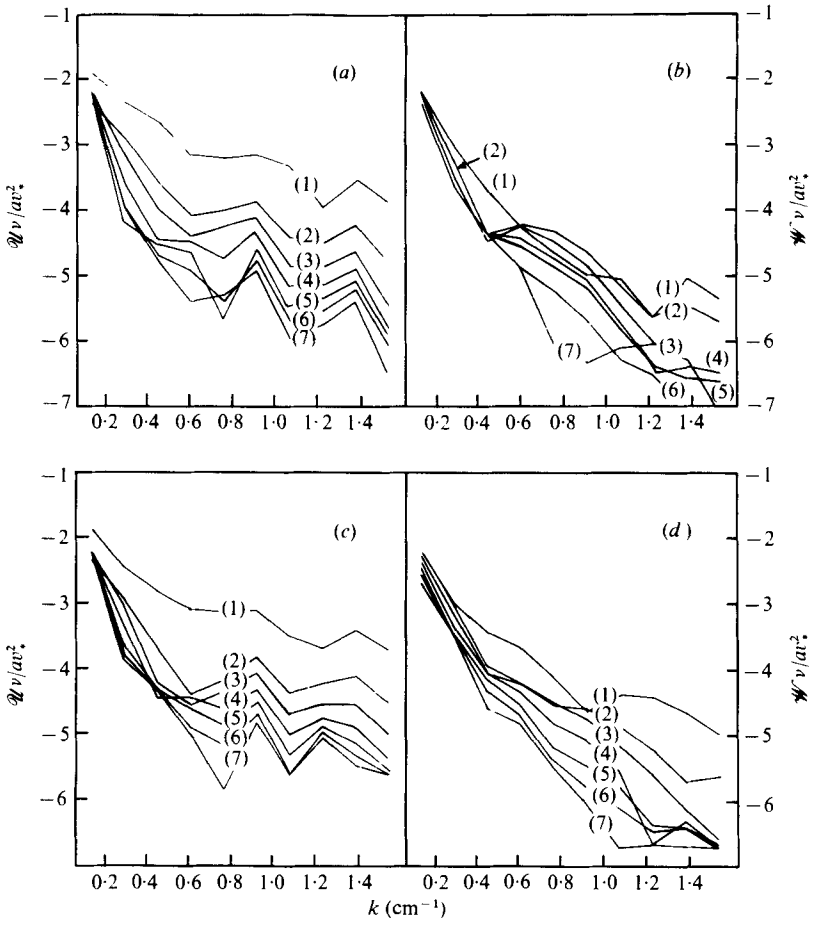

FIGURE 4. Amplitudes of the air velocity modes normalized by av_*/ν at different heights z for $v_* = 8{\cdot}33$ cm/s. (*a*), (*b*) $t = 2{\cdot}5$ s, (*c*), (*d*) $t = 5{\cdot}0$ s. (1) $z = 1{\cdot}25$ cm, (2) 2·25 cm, (3) 3·25 cm, (4) 4·25 cm, (5) 5·25 cm, (6) 6·25 cm, (7) 7·25 cm.

On average, the absolute value of the wind-induced momentum flux is 20 times smaller than that of the turbulent momentum flux. The variation with height of $k\partial u/\partial\zeta$ is largely compensated for by the term $\overline{u\tilde{w}}$. The term $\overline{p\eta_x}$ changes very little. It should be emphasized here that in the case of a considerably smaller vertical step size the ratio of the momentum flux components at the surface may vary. It can be assumed intuitively that the vertical step at the surface must at any rate be one order of magnitude smaller than the estimate of the critical-layer height. This required a non-uniform vertical step decreasing near the surface. This can be achieved by use of the vertical co-ordinate $\ln|\zeta|$ but this leads to significant complication of the numerical scheme.

A spectral analysis of the predicted velocity fields permits investigation of the vertical distribution of phases and amplitudes of the main wave-induced perturbation modes. The results of such an analysis for three situations together with similar experimental data obtained by Stewart are given in figures 7(*a*)–(*c*). Transition from the ζ to the z co-ordinate was performed by linear interpolation. All the results show

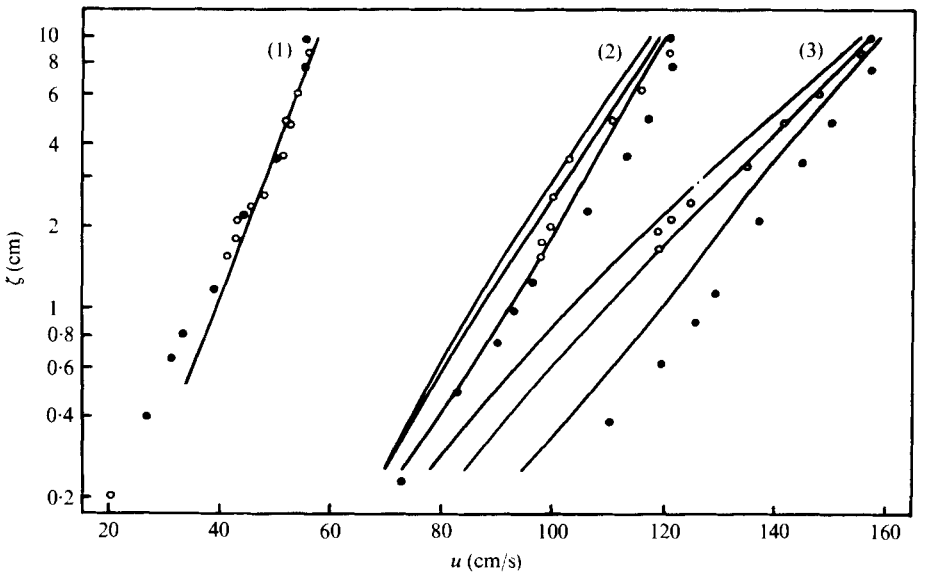

FIGURE 5. Wind velocity distribution in terms of ζ: (1) $v_* = 3{\cdot}36$ cm/s, (2) $v_* = 6{\cdot}71$ cm/s, (3) $v_* = 8{\cdot}33$ cm/s. The curves correspond to predicted wind velocities. In groups 2 and 3, the left-hand curve is above a trough, the right-hand curve is above a crest and the middle curve is averaged over $0 \leqslant \zeta \leqslant 1$. In group 1, these curves are coincident. The points are Stewart's (1970) measurements: ○, above a trough; ●, above a crest.

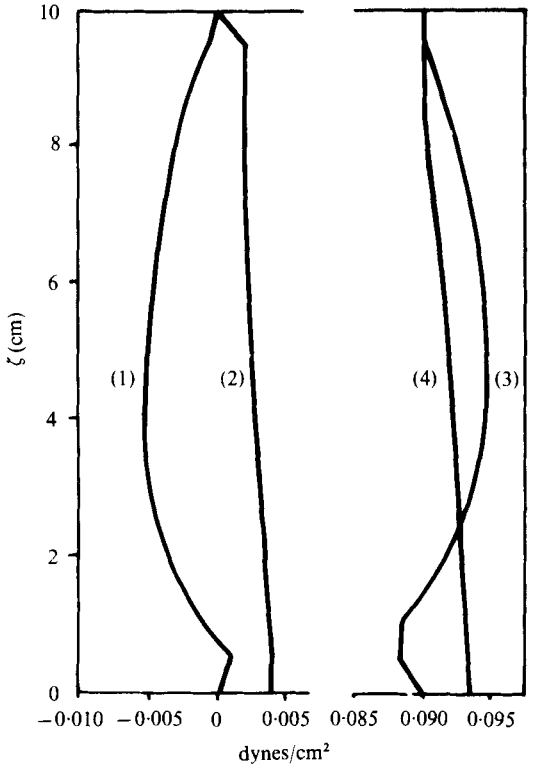

FIGURE 6. Friction component profiles in terms of ζ for $\zeta > 0$ [see (26)]. $v_* = 8{\cdot}33$ cm/s. (1) $\overline{u\tilde{w}}$. (2) $\overline{p\tilde{h}_x}$. (3) $k\,\partial u/\partial\zeta$. (4) The sum of (1)–(3). Positive values correspond to a downward momentum flux.

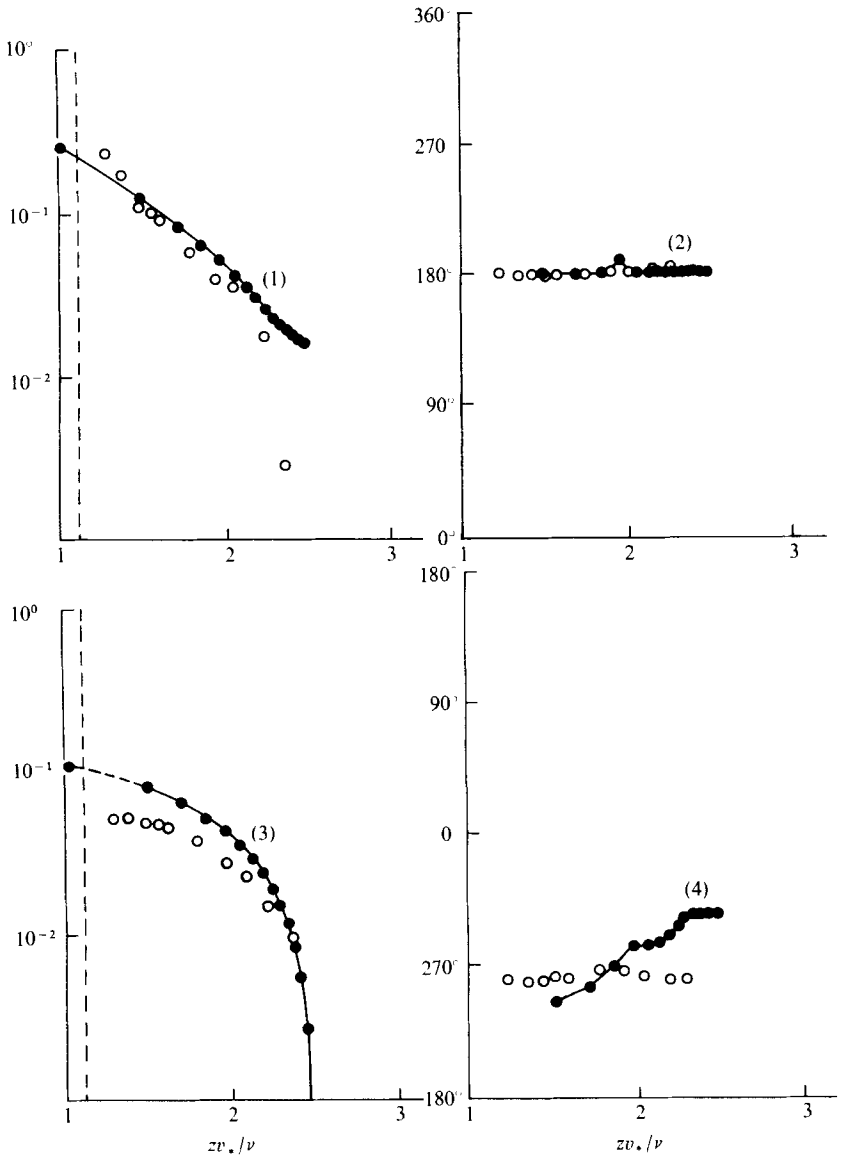

FIGURE 7 (*a*). For legend see p. 577.

that the computation simulates satisfactorily the order of magnitude and some other features of the velocity field above waves. The appreciable deviations in the upper part of the profile of $\mathscr{U}$ in figure 7(*a*) ($v_* = 3{\cdot}36$ cm/s) can, apparently, be explained by the fact that the last experimental point is outside the boundary layer.

Experimental data do not confirm a deep minimum in $\mathscr{U}$ in the neighbourhood of the critical layer for $v_* = 6{\cdot}71$ cm/s (figure 7*b*). This minimum is not so pronounced for $v_* = 8{\cdot}33$ cm/s (figure 7*c*). The difference between these results is probably due to poor vertical resolution and poor location of the real minimum relative to the nodes of the finite-difference grid. Incidentally, this remark may also apply to experimental

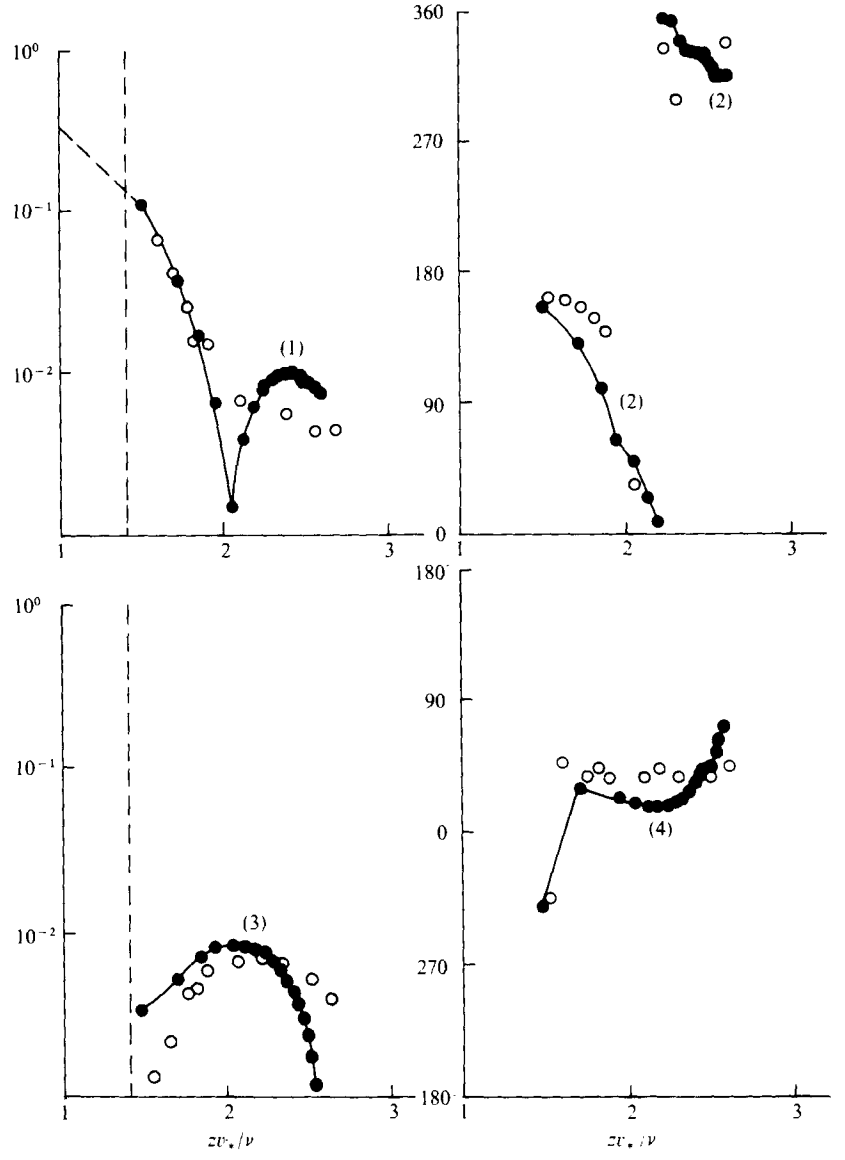

FIGURE 7 (*b*). For legend see next page.

data. Interpolation is responsible for certain errors in the computation. It is remarkable that in the region of the minima the curves are in better agreement with Davis's (1970) theoretical results used by Stewart. Generally, the phase shift is consistent with experiment.

Examples of the instantaneous velocity fields, pressure and turbulent energy for $v_* = 8{\cdot}33$ cm/s at $t = 5{\cdot}0$ s are given in figures 8 and 9. In the air, the pressure variations appeared to be of the same order of magnitude to the accuracy adopted in the iteration scheme of the pressure calculation, therefore the field $p(x, \zeta, t)$ incorporates dynamically insignificant single-step perturbations. In figure 9 (*a*), these perturbations

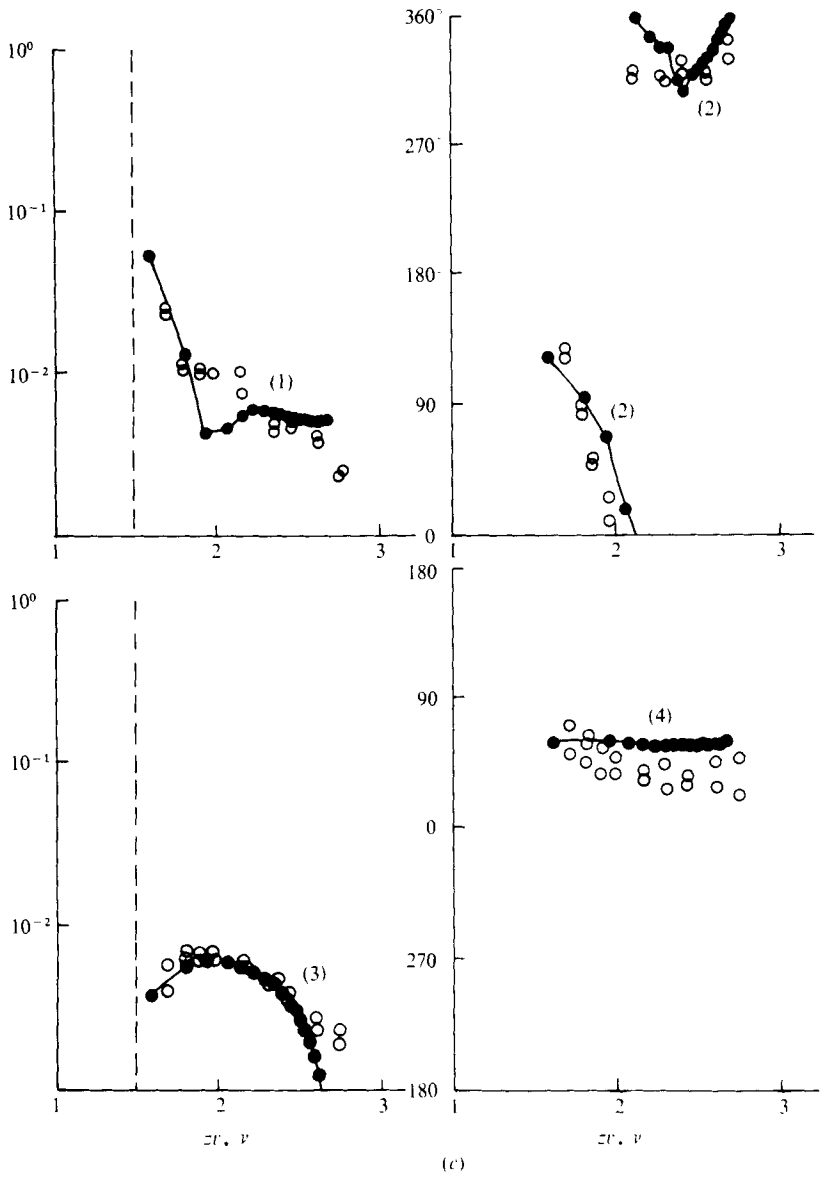

FIGURE 7. Instantaneous profiles of the non-dimensional amplitudes and phases as functions of the non-dimensional height zv_*/ν at $t = 5$. (1), (2) Amplitudes and phases of the longitudinal velocity component. (3), (4) Amplitudes and phases of the vertical velocity component. ●, calculated; ○, experimental; – – –, height of a crest. (*a*) $v_* = 3{\cdot}36$ cm/s, (*b*) $v_* = 6{\cdot}71$ cm/s, (*c*) $v_* = 8{\cdot}33$ cm/s.

are smoothed. For reasons not yet understood there usually occurred a small increment in the pressure field p for $\zeta > 0$ except at the upper level, where $p = 0$. In the situation presented in figure 9(*a*), this increment is equal to 0·039 N/m². The figure shows deviations from this value. The discontinuity in the contours near the surface in figure 8 corresponds to the region of large gradients in the parameterized boundary layer.

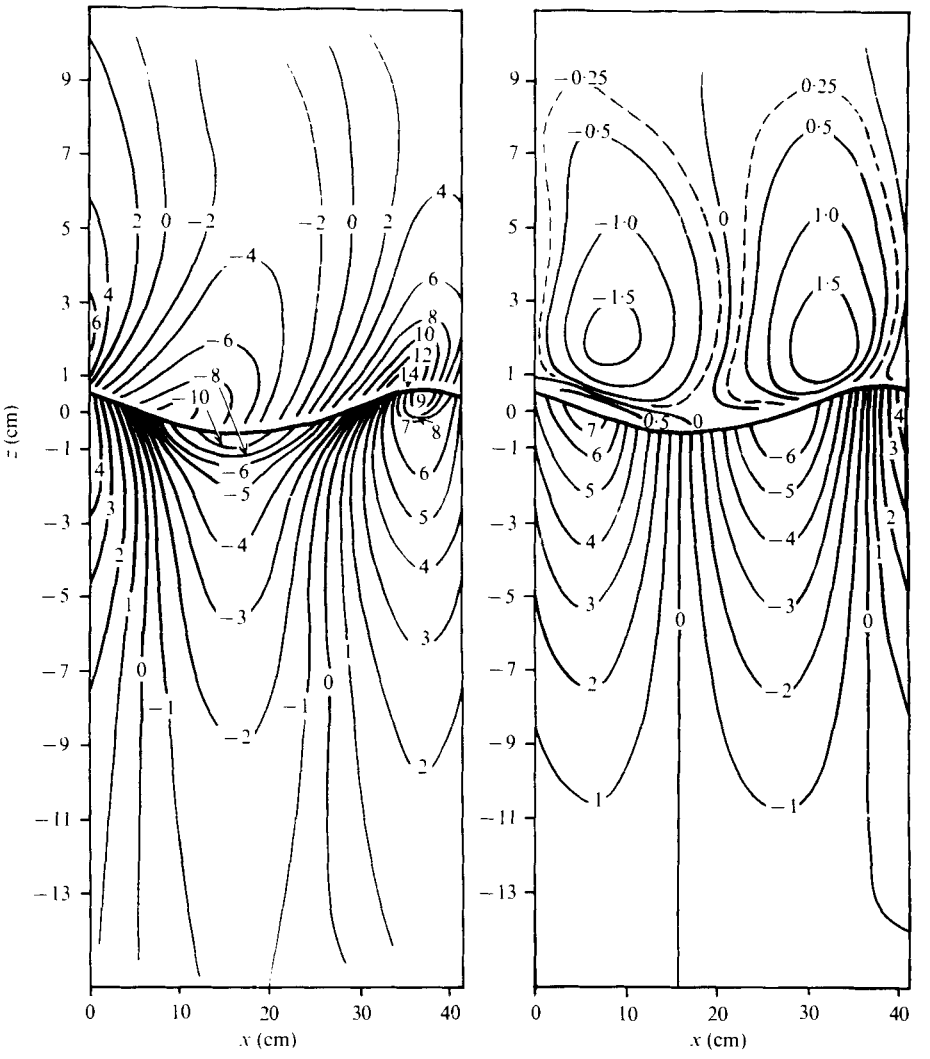

FIGURE 8. Velocity distribution. $v_* = 8{\cdot}33$ cm/s, $t = 5$ s. (*a*) u component, (*b*) w component. In (*a*), deviations from the mean value in terms of ζ over the period are given in place of the net velocity. The mean velocity profile is shown in figure 5.

7. Conclusion

What might seem a formal technique – incorporation of a moving system of coordinates – turns out ultimately to be of practical value because averaging the equations in terms of ζ leads to results amenable to a straightforward interpretation. The undesirable property of ζ, namely unsteadiness, does not appear to be very significant because the differences between ζ and z are attenuated at a reasonable distance from the interface. This effect is due to a reduction with height in all gradients and vanishing of the statistical relationship of the velocity and pressure deviations to the slopes and the velocity of the surface motion. Use of ζ and application of the G-averaging over an ensemble of similar wave situations do not necessitate presentation of the variables as the sum of wave and turbulent components.

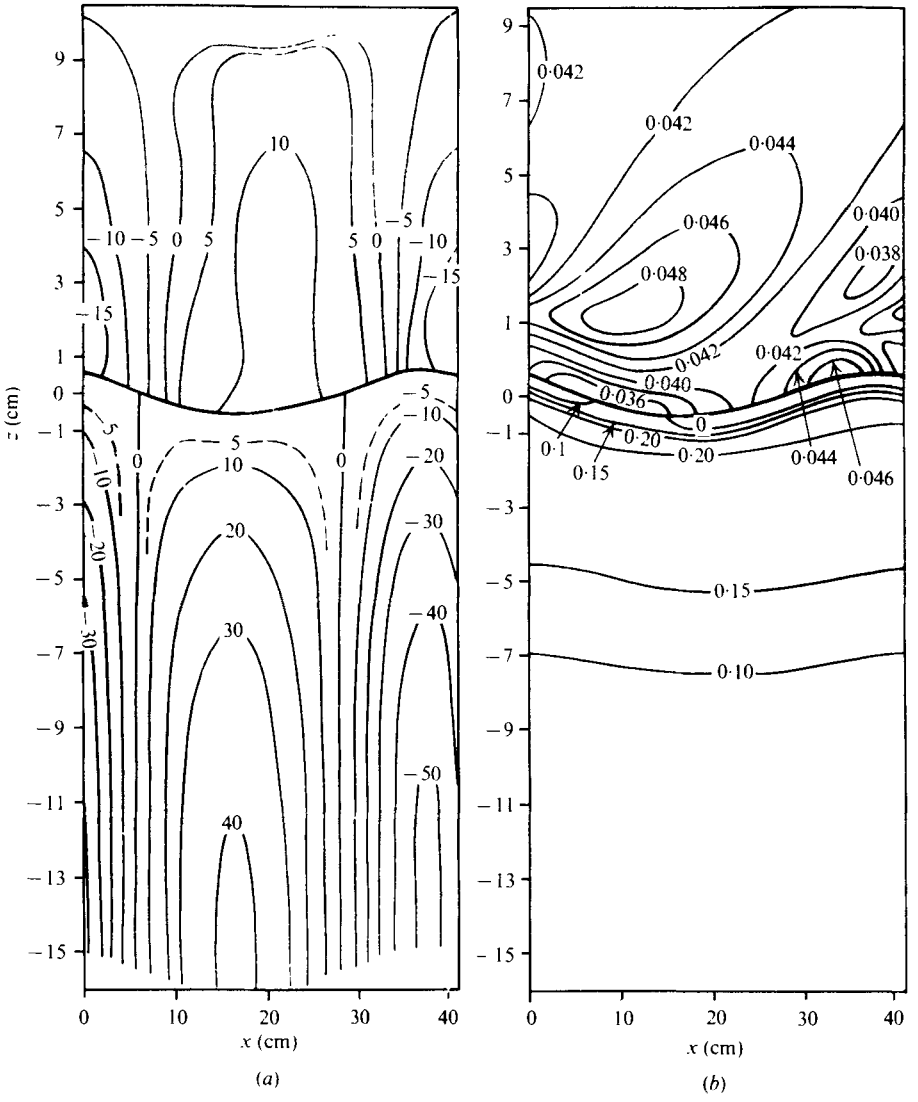

FIGURE 9. Pressure and turbulent energy distribution. $v_* = 8{\cdot}33$ cm/s, $t = 5$ s. (*a*) Pressure: $p - 0{\cdot}039$ [(N/m^2) $\times 10^{-3}$] for $\zeta > 0$; p (N/m^2) for $\zeta < 0$ (for $\zeta > 0$, p has been smoothed). (*b*) Turbulent energy (k/ms) (for $0 < \zeta < 1$ cm the height scale has been stretched).

The objective of the mathematical modelling of wind-induced perturbations is the numerical modelling of the evolution of the wave spectrum owing to wind. The foregoing results do not permit the application of the proposed model without restrictions, but they do not remove the motivation for further steps. Numerically, simulation of wind-induced perturbations is no more laborious a task than simulation of the dynamic regime of the atmosphere (Smagorinsky 1974), because to obtain a quasi-steady dynamic regime with approximately the same number of the degrees of freedom in either case it is necessary to use 10^5–10^6 time steps.

It might be interesting in a subsequent analysis to investigate the possibilities

offered by a number of modifications and improvements. Of these, the first might be an attempt to connect the numerical approach for the air to the analytical description of waves (this idea was suggested to the author by K. Hasselmann in a private discussion).

The proposed scheme may be improved by incorporation of a flow function which allows grid compression near the interface, where the energy flux towards the water is formed. An effective improvement might be achieved by writing the variables as Fourier series with amplitudes and phases dependent on the vertical co-ordinate.

In some respects, the proposed numerical model is close to that used by Taylor, Gent & Keen (1976), Gent & Taylor (1976, 1977) and Gent (1977), who performed very careful calculations of the dynamic structure of the flow above waves through reduction to a steady problem. Unfortunately, these results became available only after this paper had been completed. Most of the results above are extremely useful for further development of a mathematical model of wind-induced waves. A more thorough parameterization of water surface roughness seems to be feasible.

The author is indebted to Prof. V. M. Brekhovskikh, Prof. A. S. Monin, Prof. G. I. Barenblatt, Prof. K. Hasselmann and Dr S. A. Kitaigorodsky for valuable discussions of the problems of simulating wind-induced perturbations. The author is also grateful to Prof. J. Sundermann and Dr B. A. Kagan for very important comments made after reading the manuscript and wishes to extend his thanks to Mr E. V. Popov for assistance in preparing the English version of the paper and to Miss T. A. Babayeva for drafting the figures.

Appendix. The numerical scheme

A grid with horizontal and vertical spacings Δx and $\Delta\zeta$ was used to solve (18) and (21) numerically. Both the velocity components u and w as well as turbulent energy e were evaluated at the centre of the cell while the pressure was evaluated at its corners. The level η was calculated at the corners located nearest the interface (figure 10).

Equations (18) and (21) can be written in the form

$$u_t = -\rho^{-1}p_x + \eta_x\rho^{-1}p_\zeta + F_u, \tag{A 1}$$

$$w_t = -\rho^{-1}p_\zeta + F_w, \tag{A 2}$$

$$u_x + (w - \eta_x u)_\zeta = 0, \tag{A 3}$$

$$\eta_t = w_0 - u_0\eta_x, \tag{A 4}$$

$$e_t = (-\tilde{u}e + ke_x)_x + (-\tilde{w}e + ke_\zeta)_\zeta + k(u_x^2 + u_\zeta^2 + w_x^2 + w_\zeta^2) - \epsilon, \tag{A 5}$$

where

$$\tilde{w} = w - \eta_t - \eta_x u, \tag{A 6}$$

$$F_u = (-\tilde{u}u + ku_x + g_1\eta)_x + (-u\tilde{w} + ku_\zeta)_\zeta, \tag{A 7}$$

$$F_w = (-\tilde{u}w + kw_x)_x + (-w\tilde{w} + kw_\zeta)_\zeta. \tag{A 8}$$

The operators used to differentiate a scalar field C, say, are given by

$$\left.\begin{aligned} G^x(C) &= (C_{i+1,j} + C_{i+1,j+1} - C_{i,j} - C_{i,j+1})/(2\Delta x) - \eta_x^i(C_{i,j+1} \\ &\qquad + C_{i+1,j+1} - C_{i,j} - C_{i+1,j})/(2\Delta\zeta), \\ G^\zeta(C) &= (C_{i,j+1} + C_{i+1,j+1} - C_{i,j} - C_{i+1,j})/(2\Delta\zeta), \end{aligned}\right\} \tag{A 9}$$

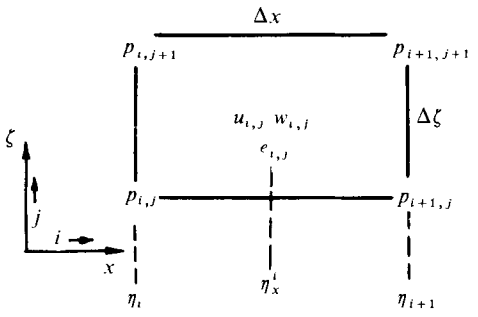

FIGURE 10. Finite-difference grid.

while the divergence operator applied to a vector field (U, W), say, is given by

$$D(U, W) = G^x(U) + G^\zeta(W). \tag{A 10}$$

Using (A 9) and (A 10), the finite-difference equations corresponding to (A 1)–(A 3) yield

$$(u^{t+1} - u^t)(\Delta t)^{-1} = -\rho_j^{-1} G^x(p) + F_u^{i,j}, \tag{A 11}$$

$$(w^{t+1} - w^t)(\Delta t)^{-1} = -\rho_j^{-1} G^\zeta(p) + F_w^{i,j}, \tag{A 12}$$

$$D(u, w) = 0. \tag{A 13}$$

Applying the operator D to the vector field (u^{t+1}, w^{t+1}) gives the finite-difference equation defining p:

$$D(\rho^{-1}G^x(p), \rho^{-1}G^\zeta(p)) = D(F_u + u^t(\Delta t)^{-1}, F_w + w^t(\Delta t)^{-1}). \tag{A 14}$$

Equation (A 14) is solved by the over-relaxation interaction method. The boundary values $p_{i,0}$ are found by substitution of the boundary conditions $u_{i,0} = w_{i,0} = 0$ into (A 11) and (A 12). The iteration process was terminated when the condition

$$\max_{i,j} |\delta p_{i,j}[|p_{ij}| + \rho_{i,j}\Delta\zeta(|F_u^{i,j}| + |F_w^{i,j}|)]^{-1}| < \mu \tag{A 15}$$

was satisfied ($\delta p_{i,j}$ is the iteration pressure increment). μ was usually chosen as 10^{-2}.

Using the continuity equation (A 3) it is possible to write (A 4) in the following finite-difference form:

$$\eta_i^{t+1} = \eta_i^t - \Delta t \Delta\zeta \Delta x^{-1} \sum_{j+1}^{k} (u_{i,j} - u_{i-1,j}), \tag{A 16}$$

where summation is performed over the region $\zeta < 0$.

Approximation of (A 7) and (A 8) gives

$$\begin{aligned} F_u^{i,j} = {} & [-\tilde{u}_{i+\frac{1}{2},j} u_{i-\frac{1}{2},j} + \tilde{u}_{i-\frac{1}{2},j} u_{i-\frac{1}{2},j} + k_{i+\frac{1}{2},j}(u_{i+1,j} - u_{i,j})(\Delta x)^{-1} \\ & - k_{i-\frac{1}{2},j}(u_i - u_{i-1})(\Delta x)^{-1} + g_1(\eta_{i+1} - \eta_i)](\Delta x)^{-1} \\ & + [-u_{i,j+\frac{1}{2}} \tilde{w}_{i,j+\frac{1}{2}} + u_{i,j-\frac{1}{2}} \tilde{w}_{i,j-\frac{1}{2}} + k_{i,j+\frac{1}{2}}(u_{i,j+1} - u_{i,j})(\Delta\zeta)^{-1} \\ & - k_{i,j-\frac{1}{2}}(u_{i,j} - u_{i,j-1})(\Delta\zeta)^{-1}](\Delta\zeta)^{-1}, \end{aligned} \tag{A 17}$$

$$\begin{aligned} F_w^{i,j} = {} & [-\tilde{u}_{i+\frac{1}{2},j} w_{i+\frac{1}{2},j} + \tilde{u}_{i-\frac{1}{2},j} w_{i-\frac{1}{2},j} + k_{i+\frac{1}{2},j}(w_{i+1,j} - w_{i,j})(\Delta x)^{-1} \\ & - k_{i-\frac{1}{2},j}(w_{i,j} - w_{i-1,j})(\Delta x)^{-1}](\Delta x)^{-1} \\ & + [-w_{i,j+\frac{1}{2}} \tilde{w}_{i,j+\frac{1}{2}} + w_{i,j-\frac{1}{2}} \tilde{w}_{i,j-\frac{1}{2}} + k_{i,j+\frac{1}{2}}(w_{i,j+1} - w_{i,j})(\Delta\zeta)^{-1} \\ & - k_{i,j-\frac{1}{2}}(w_{i,j} - w_{i,j-1})(\Delta\zeta)^{-1}](\Delta\zeta)^{-1}, \end{aligned} \tag{A 18}$$

where

$$u_{i+\frac{1}{2},j} = \tfrac{1}{2}(u_{i,j} + u_{i+1,j}),$$

$$\tilde{u}_{i+\frac{1}{2},j} = \tfrac{1}{8}(u_{i+1,j+1} + 2u_{i+1,j} + u_{i+1,j-1} + u_{i,j+1} + 2u_{i,j} + u_{i,j-1}),$$

$$w_{i,j+\frac{1}{2}} = \tfrac{1}{2}(w_{i,j} + w_{i,j+1}),$$

$$\begin{aligned}\tilde{w}_{i,j+\frac{1}{2}} = {} & \tfrac{1}{8}(w_{i-1,j} + w_{i-1,j+1} + 2w_{i,j} + 2w_{i,j+1} + w_{i+1,j} + w_{i+1,j+1}), \\ & - \tfrac{1}{2}(\eta_t^{i+1} + \eta_t^i) - \tfrac{1}{8}(\eta_x^i + \eta_x^{i-1})(u_{i-1\ j} + u_{i-1,j-1} + u_{i,j} + u_{i,j+1}), \\ & - \tfrac{1}{8}(\eta_x^{i-1} + \eta_x^i)(u_{i,j} + u_{i,j+1} + u_{i+1,j} + u_{i+1,j+1}).\end{aligned}$$

The terms in (A 17) and (A 18) describing the momentum transport through the interface $\zeta = 0$ by viscous forces are calculated according to (11). The forms of (A 17) and (A 18) ensure convergence of $\tilde{w}$ to zero at the interface [see the appropriate remark concerning (3)]. Subsequent construction of the finite-difference scheme for (A 5) is obvious. The time derivatives and all of the foregoing calculations were approximated using directional differences. One iteration was used every other step for the entire problem.

REFERENCES

Barnett, T. P. & Kenyon, K. E. 1975 Recent advances in the study of wind waves. *Rep. Prog. Phys.* **38**, 667–729.

Chalikov, D. V. 1976 A mathematical model of wind waves. *Dokl. Akad. Nauk SSSR* **197**, 1083–1086.

Davis, R. E. 1970 On the turbulent flow over a wavy boundary. *J. Fluid Mech.* **42**, 721–732.

Gent, P. R. 1977 A numerical model of the air flow above water waves. Part 2. *J. Fluid Mech.* **82**, 349–369.

Gent, P. R. & Taylor, P. A. 1976 A numerical model of the air flow above waves. *J. Fluid Mech.* **77**, 105–128.

Gent, P. R. & Taylor, P. A. 1977 A note on 'separation' over short wind waves. *Boundary-Layer Met.* **11**, 65–87.

Kitaigorodsky, S. A. 1970 *The Physics of Air–Sea Interaction.* Leningrad: Gidrometeoizdat.

Miles, J. W. 1957 On the generation of surface waves by shear flows. *J. Fluid Mech.* **3**, 185–204.

Monin, A. S. & Yaglom, A. M. 1971 *Statistical Fluid Mechanics.* MIT Press.

Phillips, O. M. 1957 On the generation of waves by turbulent wind. *J. Fluid Mech.* **2**, 417–445.

Phillips, O. M. 1958 The equilibrium range in the spectrum of wind-generated waves. *J. Fluid Mech.* **4**, 426–434.

Phillips, O. M. 1966 *The Dynamics of the Upper Ocean.* Cambridge University Press.

Smagorinsky, J. 1974 Global atmospheric modelling and the numerical simulation of climate. In *Weather and Climate Modification*, pp. 633–686. Wiley.

Stewart, R. H. 1970 Laboratory studies of the velocity field over deep-water waves. *J. Fluid Mech.* **42**, 733–754.

Taylor, P. A., Gent, P. R. & Keen, J. M. 1976 Some numerical solutions for turbulent boundary-layer flow above fixed, rough, wavy surfaces. *Geophys. J. Roy. Astr. Soc.* **44**, 177–201.

Zilitinkevich, S. S. 1970 *The Dynamics of the Atmospheric Boundary Layer.* Leningrad: Gidrometeoizdat.